Diffusion-driven evaporation of sessile drops

2005 J. Phys.: Condens. Matter 17 S4213

(http://iopscience.iop.org/0953-8984/17/49/015)

INSTITUTE OF PHYSICS PUBLISHING JOURNAL OF PHYSICS: CONDENSED MATTER

J. Phys.: Condens. Matter **17** (2005) S4213–S4227 doi:10.1088/0953-8984/17/49/015

Diffusion-driven evaporation of sessile drops

C Poulard, G Guéna and A M Cazabat[1]

Collège de France, 11 place Marcelin Berthelot, 75231 Paris Cedex 05, France

Received 30 June 2005, in final form 20 October 2005
Published 25 November 2005
Online at stacks.iop.org/JPhysCM/17/S4213

Abstract

The evaporation of wetting drops deposited on a substrate at thermal equilibrium under normal atmosphere is discussed. The evaporation rate appears to be controlled by the stationary diffusion of vapour molecules in the gas phase. Experiments with alkanes and water drops are fairly well accounted for by an isothermal model, taking into account the specific properties of thin films.

(Some figures in this article are in colour only in the electronic version)

1. Introduction

The study of aerosol droplets evaporating in normal atmosphere is a long story, going back to Maxwell and Langmuir [1, 2]. At first sight, one might expect the evaporation rate of a spherical drop to be proportional to the drop area, and therefore the drop radius to decrease linearly with time. This is actually the case in vacuum, or more generally in situations where the mean free path of the vapour molecules in the gas phase is large with respect to the drop size [3]. In contrast, experiments usually show that the evaporation rate of aerosol droplets under quiet, normal atmosphere is proportional to the drop radius [3–9]. More recently, experiments by Deegan in Chicago [10–12] with evaporating sessile drops induced a renewed interest in the problem.

Unlike the case of heat exchangers and heated substrates [13–15], where the system is driven far from equilibrium by an imposed temperature difference, the evaporating drop is initially at the same, uniform temperature as the gas phase and (if any) the substrate. Evaporation may induce temperature changes, but one can find conditions where the evaporation is slow enough for these thermal effects to be negligible. In the same way, one expects, again for slow enough evaporation rate, the gas phase just above the free liquid interface to be practically at equilibrium with it [3]. Far from the drop, the concentration of vapour in the atmosphere is fixed at some equilibrium value.

What ‘slow enough’ means requires discussion.

If the gas phase is at rest, the transport of vapour molecules proceeds by diffusion. A first assumption is that the interface normal velocity due to evaporation is much smaller than the velocity scale associated with the building up of the concentration profile in the

[1] Author to whom any correspondence should be addressed.

atmosphere. This means that stationary diffusion is a good approximation for slowly evaporating liquids [16].

A second assumption is that the rate-limiting step for evaporation is the diffusive relaxation of the vapour immediately above the free liquid surface, and not the transfer rate of molecules across the liquid–vapour interface [3, 4, 16, 17]. Typical values of transfer rates are 10^{-10} s, while the characteristic time of diffusion over a distance d is d^2/D, where D is the diffusion coefficient of vapour molecules in air. For water vapour in a normal atmosphere, $D \approx 2.4 \times 10^{-5}$ m^2 s^{-1}, and the two timescales become comparable for distances ≈ 0.1 μm, which is also the mean free path of water molecules.

Therefore, the slow evaporation of macroscopic aerosol drops in a quiescent atmosphere is controlled by the stationary diffusion of the evaporating molecules in the gas phase, with simple, constant boundary values $c_{\mathrm{sat}}(T)$ at the interface ($c_{\mathrm{sat}}(T)$ being the saturation value at the temperature T of the surroundings) and c_∞ at infinity. As pointed out by Maxwell and Langmuir, the concentration in the evaporation problem obeys $\Delta c = 0$, and solutions of the equivalent electrostatic problem $\Delta \Phi = 0$ where Φ is the potential are well known [1, 2, 18, 19]. For instance, at time t, the concentration at distance r from the centre of a slowly evaporating spherical aerosol droplet of radius $R(t)$ reads ($r \geqslant R$)

$$c\,(R, t) - c_\infty = (c_{\mathrm{sat}} - c_\infty)\frac{R(t)}{r}.$$

The evaporating rate (in mass if the concentration is mass per unit volume) is [2, 3]

$$\frac{\mathrm{d}m}{\mathrm{d}t} = -4\pi D(c_{\mathrm{sat}} - c_\infty)R(t).$$

If ρ is the constant mass concentration of the liquid

$$R^2 = \frac{2D(c_{\mathrm{sat}} - c_\infty)}{\rho}(t_0 - t).$$

This accounts well for the experimental results obtained with aerosols.

Here, the evaporation velocity is $\frac{\mathrm{d}R}{\mathrm{d}t}$; the velocity scale for diffusion is $\frac{D}{R}$. The ratio is $\frac{c_{\mathrm{sat}}}{\rho}$, much smaller than unity for slowly evaporating liquids ($\approx 10^{-4}$ for octane and 2×10^{-5} for water at 25 °C). Therefore, the assumption of stationarity is well supported.

The problem is more complex with sessile drops. Then the electrostatic analogy is a symmetric, biconvex conducting lens put at a given potential Φ_{s} [10–12]. The electric field diverges at the perimeter of the lens, which causes no specific difficulty in electrostatics, but questions the relevance of the electrostatic analogy in the evaporation problem.

The use of the electrostatic analogy was first proposed by Deegan *et al* in the case of sessile drops with pinned contact line, in their analysis of rings left by evaporating coffee drops [10]. The radius $R(t)$ of the wetted spot is constant, and the loss of volume proceeds through a mere decrease of the contact angle. The theoretical analysis is still going on, noticeably for the study of deposit growth from colloidal dispersions, which is relevant for industrial applications [11, 12]. The complete formulae are rather complex. They become simple only when the contact angle θ of the sessile drop is small, $\theta \ll 1$. Then the electrostatic analogy is a disc at constant potential. This is the situation encountered in complete wetting, where the measured contact angles are of the order of 10^{-2} rad.

The assumption of a diffusion driven evaporation process has to be reconsidered at the edge of the drop. Moreover, in the specific case of complete wetting, the assumption of stationarity also needs to be discussed, because the contact line velocity is much larger than the velocity normal to the interface. This mere effect leads the stationarity condition to become $\frac{c_{\mathrm{sat}}}{\theta\,\rho} \ll 1$ at the contact line, instead of $\frac{c_{\mathrm{sat}}}{\rho} \ll 1$. In fact, the condition is still largely fulfilled for the liquids considered here.

However, what happens in the vicinity of the contact line is complex. As a matter of fact, the contact angle of a receding, non-volatile liquid is zero. Finite, although small, contact angles are observed because the liquid is volatile, and specifically because the evaporation rate increases at the edge of the drop [20–23]. Actually, evaporation rate is a balance between molecules leaving the liquid and molecules coming back from the gas phase. At the edge of the drop, the probability for a molecule from the gas phase to reach the liquid interface decreases. The corresponding increase of the evaporation rate induces a significant flow of the liquid towards the edge, which is at the origin of the characteristic coffee rings, and increases the contact angle.

The first study of the dynamics of an evaporating wetting drop is probably due to Deegan himself. The time dependence $R(t)$ of the radius of a water drop evaporating on mica can be found in [11]. During the drop retraction, the trend is $R(t) \propto (t_0 - t)^y$, with $y \approx 0.65$. Such an exponent differs significantly from the one ($y = 0.5$) measured in aerosols. Bearing in mind the possible limitations of the models, it is interesting to check if this exponent is the rule for sessile drops, or if water is specific for some physico-chemical reason.

All these questions are the motivation of our long-lasting investigations on the dynamics of evaporating drops [24–26]. The present paper presents a brief summary of our previous work, recent experimental studies, and a complete analysis of the models available at the present time.

2. Experimental study of evaporating wetting drops

2.1. Materials and methods

The liquids used are alkanes, from nonane to hexane (Aldrich, >99% pure), and water (ultrapure, milliQ, from several origins).

Drops with controlled volume are deposited on the solid substrate. The radius $R(t)$ of the wetted spot increases first, because the liquid wets the substrate, then goes to a maximum, and later on decreases to zero, because of the evaporation going on. The dynamics is followed under a microscope in normal atmosphere, with protection against air draughts. A low magnification is used for the measurement of the radius, which is done with the entire drop in the field of the microscope. In contrast, the measurement of contact angle from equal thickness interference fringes at the drop's edge requires a high magnification.

This is a potential cause of artefacts. One must be aware, especially at high magnification, of the possible heating due to the focused microscope beam. Note that we use 'extra long working distance' objectives to keep the surface of the objective far from the drop, and avoid any significant confinement of the atmosphere on top of it. However, shifting the substrate to keep the moving drop's edge in the field of the microscope has to be done smoothly, not to induce convection in the gas phase.

As water vapour is lighter than air, buoyancy driven convection is possible above evaporating water drops, in contrast with alkanes.

A different set-up is available, where the drop plays the role of either a mirror, or a flat-convex lens. Details can be found elsewhere [27]. The set-up provides a direct measurement of focal lengths, which allows us to obtain the curvature radius at the centre of the drop, and also the ratio $\frac{R}{\theta}$ at the edge. Contact angle and radius can also be deduced separately by analysing the various emerging beams. The closest optical piece is located several centimetres from the drop, and the source is a widened, parallel, 5 mW laser beam, 1 cm in diameter. Therefore neither confinement nor heating are expected with that set-up, referred to as 'laser set-up' in the following.

The time t_0 where the drop disappears has to be measured precisely. This allows us to plot radius and angle as a function of the time interval $t_0 - t$ in a log–log scale. It is worth noting that the scattering of data is increased for small radius and angle with respect to a linear plot, but the log–log plot is the most relevant one for the comparison with theoretical analyses.

The substrates are oxidized silicon wafers, made water wettable by proper cleaning. The native oxide layer is typically 2 nm thick. According to the cleaning procedure, the silica surface exhibits a variable relative amount of high energy silanol groups (Si–OH), and low energy siloxane bridges (Si–O–Si). While most cleaning procedures are equivalent for alkanes, this is not the case with water. The 'Piranha' solution (one-third H_2O_2, two-thirds H_2SO_4) provides fairly reproducible hydrophilic substrates. The UV–ozone cleaning [28] also gives water wettable substrates, slightly less hydrophilic.

2.2. *Experimental results with alkane drops*

Some of the results obtained with alkanes are available in previous publications [24–27] and will be briefly summaried. Alkanes have been chosen as being non-polar liquids without specific interaction with the substrates.

During the receding motion, the radius obeys well defined power laws $R(t) \propto (t_0 - t)^y$. The exponent y increases regularly from 0.44 for nonane to 0.48 for hexane.

The behaviour of the angle is more complex. Three stages can be defined, the better separated in time the lighter the alkane is. During the first stage, the angle decreases rapidly while the radius first increases (during spreading) then reaches its maximum value. The second stage starts at the beginning of the retraction. The decrease of the angle is slow, fairly well described by a power law $\theta(t) \propto (t_0 - t)^x$. The exponent x decreases from nonane to hexane, and there is a simple relation $2y+x \approx 1$ between the exponents for radius and angle respectively. The last stage is again a fast decrease, with scattered data, noticeably compatible with a power law $\theta_{\text{late}}(t) \propto (t_0 - t)^{0.5}$. The values θ_0 at the beginning of the retraction can be compared for drops of similar size. The angle θ_0 increases from nonane (0.011 rad) to hexane (0.042 rad). Typical records for radius and angle for octane, obtained either with the microscope or with the laser set-up, are given in figure 1(a).

With the laser set-up, the ratio R/θ at the edge of the drop is obtained independently. A typical plot of R/θ is given in figure 1(b). The slope of the log–log plot is y–x during the second stage, and the experimental value 0.4 is in good agreement with the independent data of figure 1(a). The set-up also allows us to check if the drop shape is actually a spherical cap, by inserting masks to measure focal lengths either at the centre of the drop or at the edge. A flattening of the drops, indicated by a curvature radius in the centre larger than R/θ, is observed for drop radius larger than the capillary length; see figure 1(b). The drop shape is well accounted for by a static calculation including merely surface tension and gravity [27].

The thickness profile of the drops can be directly measured from equal thickness interference fringes during the late part of stage 2, and stage 3, where the drop radius is smaller than the capillary length. As expected, the drops are spherical caps.

2.3. *Experimental results with water drops*

Experiments with water drops were found unexpectedly difficult, especially for the measurement of angles. While the first stage does not differ significantly from the one observed with alkanes, the behaviour which follows is extremely sensitive to parameters which are not fully identified.

As previously mentioned, buoyancy-driven convection is possible in the gas phase. Noticeably, contact line instabilities are frequent during the main part of the retraction [26], especially when the wafers are cleaned with the Piranha solution.

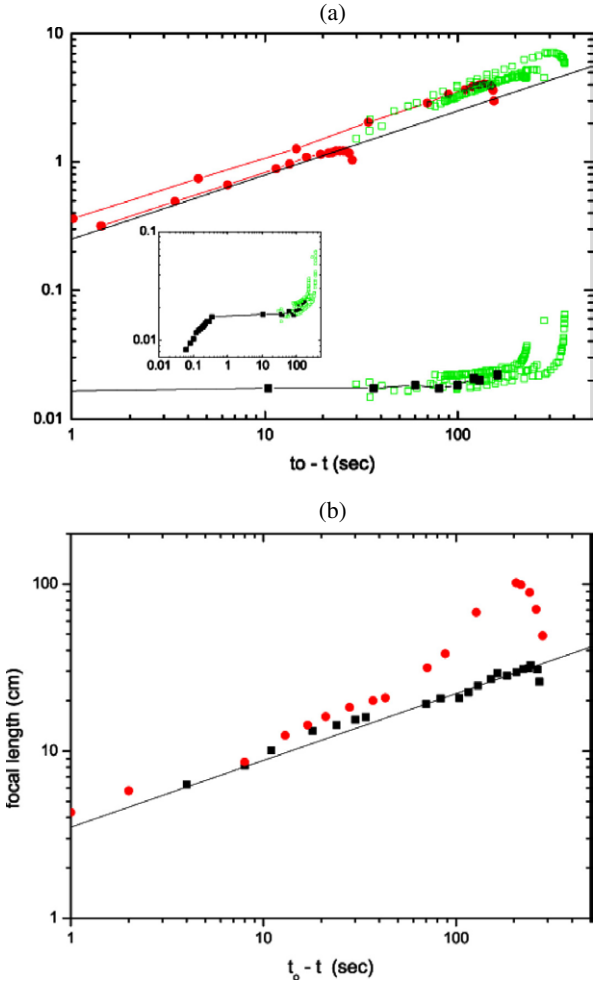

Figure 1. (a) Log–log plot of radius (mm, upper curves) and contact angle (rd, lower curves) versus time interval $t_0 - t$ for several octane drops with initial volumes between 2 and 10 μl. Microscope, full symbols; laser set-up, open squares. For the measurement of the angle with the microscope, an interference filter and an anticaloric slab have been inserted. Inset: full range variation of contact angle, including late times ($t \to t_0$). (b) Laser set-up. Log–log plot of the curvature radius in the centre (circles) and the value of R/θ at the edge (squares), both in cm, as a function of time interval $t_0 - t$ for two octane drops of same initial volume (7 μl). The two curves merge 30 s before the drops disappear; this corresponds to $R = 1.5$ mm, close to the capillary length of octane (1.8 mm). The straight line has a slope of 0.4, in good agreement with the value y–x obtained independently (see (a)).

All this suggests that both surface effects and hydrodynamic motions in the gas phase come into play.

The most convincing results were obtained recently in three different experiments involving two cleanings. Two experiments were performed under the microscope, either with UV–ozone or Piranha cleaning. Both an anticaloric plate and an interference filter were inserted to avoid any heating by the microscope beam. The third experiment was done with the laser set-up and the UV–ozone cleaning.

Measured values of the radius and angle of water drops evaporating on wafers cleaned with the UV–O_3 procedure are given in figure 2.

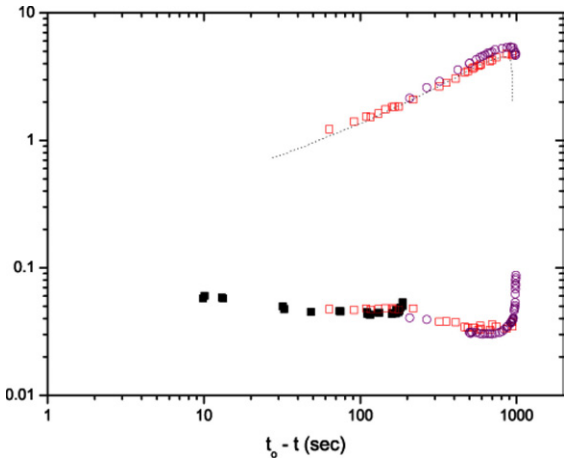

Figure 2. Water, UV–O_3 cleaning. Radius (mm, upper curves) and contact angle (rad, lower curves) for water drops of different initial volumes (between 4 and 10 μl). Microscope, dotted line for the radius, full symbols for the angle; laser set-up, open symbols. For the measurement of the angle with the microscope, an interference filter and an anticaloric slab have been inserted.

At the beginning of the retraction, a fairly well defined power law is observed for the radius, with an exponent $y \approx 0.57$, in agreement with the previous study by Deegan on a mica substrate. Later on, the scattering of the data becomes significant.

After a fast decrease, the angle increases during the second stage (i.e. the main part of the retraction), which means that the exponent x is negative. Data for radius and angle are compatible with the relation $2y + x \approx 1$.

Direct measurements of R/θ and of the curvature at the centre are reported in figure 3, in good agreement with the independent determinations of radius and contact angle given on figure 2.

The influence of the cleaning procedure is illustrated in figure 4, where the data obtained with the Piranha cleaning have been reported. The main change is observed on the contact angle, which is less with the Piranha cleaning. This means that the surface state plays a significant role. This was not expected in a complete wetting situation, where the surface energy should enter the dynamics only through logarithmic terms.

In the same way, the third stage of the life of water drops is very specific. Usually, one observes a sudden, fast increase of the angle, followed by a even faster decrease and a sort of explosion of the drop. The amplitude of the effects, and the duration of the whole process, depend drastically on the cleaning procedure [27].

3. Model of evaporating wetting drops

3.1. Model for a wetting drop

The starting point is the local conservation equation, written in the lubrication limit where the slope of the interface is small:

$$\frac{\partial h}{\partial t} + \nabla (hU) = -J(r) \tag{1}$$

h is the local thickness, hU the hydrodynamic flux, r the distance to drop axis, U the velocity averaged over the thickness, and $J(r)$ the evaporation rate.

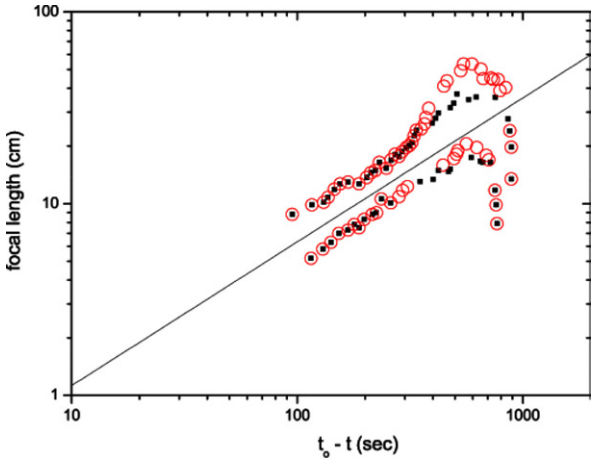

Figure 3. Water, cleaning procedure: UVO_3, laser set-up. Curvature radius in the centre (open circles) and value of R/θ at the edge (full squares), both in cm, for two drops with initial volume 5 (bottom) and 10 (top) μl respectively. The straight line has a slope 0.75, in good agreement with the value of y–x found by independent measurements (figure 2). The curves merge for a radius $R = 3.5$ mm, in fairly good agreement with the value of the capillary length (2.7 mm).

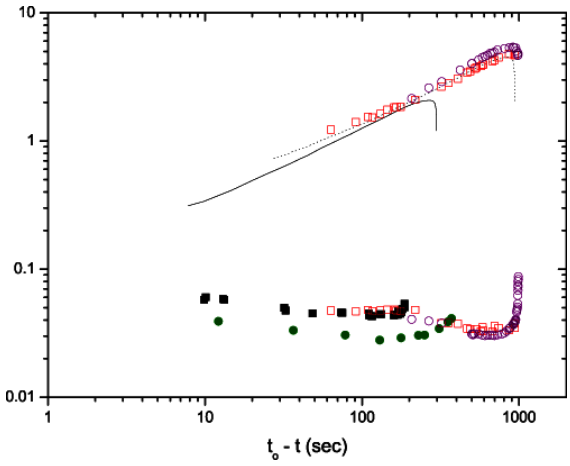

Figure 4. The same as figure 2, where the data obtained with a Piranha cleaning have been added. Radius: the Piranha cleaning corresponds to the continuous line, not very different from the data obtained with the UV–O_3 cleaning. Angle: the Piranha cleaning corresponds to the full circles, significantly below the points obtained with the UV–O_3 cleaning.

For the slow evaporation considered, there is no extra pressure due to the back-reaction of molecules passing into the gas phase. The mean velocity takes the form

$$U(h,t) = \frac{h^2}{3\eta}\nabla(\gamma\Delta h - \rho g h + \Pi(h)) + \frac{h}{2\eta}\nabla\gamma. \tag{2}$$

η is the viscosity of the liquid, γ the surface tension, ρ the density, g the acceleration of gravity and $\Pi(h)$ the disjoining pressure, which is an extra term coming into play for thin films.

As the contact angle is very small, the evaporation rate $J(r)$ can in principle be calculated using the electrostatic analogy of a flat disc kept at constant potential. At the macroscopic

scale, the electric field diverges at the disc edge, but this is no longer the case when microscopic lengths are considered.

In the same way, the evaporation rate is finite. As mentioned previously, the rate-limiting step for evaporation becomes the transfer rate of molecules at a small scale. Moreover, another rate-limiting process comes into play when a substrate is involved. It results from the properties of thin wetting films [29–31], for which the evaporation rate is less than that of bulk phases.

In any case, the evaporation rate has a finite maximum at some distance ℓ from the drop's edge and vanishes at the edge.

3.1.1. Discussion of the total evaporation rate. How to write explicitly the evaporation rate at the edge of the drop is still an open problem. This is not very serious when the contact line is pinned. As a matter of fact, the electrostatic field at the surface of a disc of radius R kept at a given potential Φ_S is perpendicular to the disc surface and is written [18]

$$E = -\frac{2\,\Phi_S}{\pi}\frac{1}{\sqrt{R^2 - r^2}}. \tag{3}$$

The flux of the field through the upper disc surface is $4\Phi_S R$. If the integral is cut at a some short distance ℓ from the edge, the result is

$$4\Phi_S R\left[1 - \sqrt{\frac{2\,\ell}{R}}\right]. \tag{4}$$

This means that, despite the divergence, the weight of the edge in the integral is small as long as $\ell \ll R$, which is the case for macroscopic drops when the contact line is pinned. Therefore, the electrostatic analogy gives a good estimate of the evaporation rate of the entire drop, whatever the precise shape of the evaporation close to the edge may be [10–12].

At this point, it is possible to explain the relation $2y+x \approx 1$ found experimentally between the exponents of radius and angle. The evaporation rate deduced from the electrostatic analogy reads

$$J(r) = \frac{j_0}{\sqrt{R^2 - r^2}} \tag{5}$$

where j_0 is an area per unit time. The integral of the conservation equation over the disc of radius R gives the rate of change of the drop volume. For $\ell \ll R$, one finds

$$\frac{\mathrm{d}V}{\mathrm{d}t} \approx -2\pi j_0 R. \tag{6}$$

In the range where the drops are spherical caps, as $\theta \ll 1$, the volume can be written as

$$V \approx \frac{\pi}{4} R^3 \theta. \tag{7}$$

During the receding motion, the radius is well fitted by a power law $R(t) \propto (t_0 - t)^y$. For spherical caps, if (6) is valid, then the angle must also be fitted by a power law $\theta(t) \propto (t_0 - t)^x$, and there is a relation $2\,y+x = 1$ between the exponents. However, no information is available at this stage on y and x separately.

3.1.2. Evaporation rate in the vicinity of the contact line. Let us proceed further and consider the dynamics of the contact line. One might expect problems at the end of the drop's life, when the radius becomes of order ℓ. This is actually the case, but the difficulties show up earlier. Actually, even if the rate of evaporation for the entire macroscopic drop is well defined as a function of the drop radius, the dynamics depends both on radius and contact angle. Depending

on the model used for describing the evaporation rate at the edge of the drop, the contact angle and the subsequent dynamics will be different.

The available models are empirical, in the sense that they still use the electrostatic formula (5) and either smooth out the divergence by mere mathematical tricks [24–26], or introduce a maximum value taken at a distance ℓ from the edge [27]. In contrast to the former ones, this latter procedure rests on physical arguments, i.e., the rate-limiting processes for evaporation.

Either the rate-limiting step is the transfer rate of molecules across the liquid–vapour interface, in which case ℓ is a constant, or it is due to the specific properties of thin films, in which case ℓ will depend on the disjoining pressure. Let us discuss this last case explicitly.

In the slow evaporation limit, and for $c_\infty = 0$, the rate of evaporation of a macroscopic film is proportional to the equilibrium concentration $c_{\rm sat}$ at saturation. For a thin wetting film on a substrate, the equilibrium concentration $c_{\rm equ}$ at the film surface is smaller than $c_{\rm sat}$ and tends to zero for vanishing film thickness [29, 30]. More precisely, the disjoining pressure can be written as

$$\Pi(h) = \frac{kT}{\varpi} \ln \frac{c_{\rm sat}}{c_{\rm equ}} \tag{8}$$

where ϖ is the volume of the molecule (270×10^{-30} m^3 for octane, ten times less for water). $\Pi(h)$ is positive for a wetting film and diverges to $+\infty$ for $h \to 0$. For alkanes, the interaction is purely dispersive and the disjoining pressure can be written as [29–31]

$$\Pi(h) = \frac{A}{6\pi h^3}. \tag{9}$$

A is the Hamaker constant for the air/alkane/silica system ($A \approx 1.7 \times 10^{-20}$ J for octane). The distance to the edge where the disjoining pressure plays a role is, for a simple dispersive interaction, of the order of $a\theta^{-2}$, where $a = \sqrt{\frac{A}{6\pi\gamma}}$ is a molecular length [31]. Therefore, it is logical to use as an upper boundary the value of the evaporation rate at a distance $\ell \approx a\theta^{-2}$ from the edge.

The important point here is the relation between ℓ and contact angle, which depends explicitly on the shape of the disjoining pressure, and has direct consequences on the dynamics.

3.1.3. Dynamics of the drop edge. The next step is to estimate the contact angle at a distance $\ell \approx a\theta^{-2}$ from the contact line, as first proposed by Benamar and co-workers in [27].

In the mean velocity,

$$U(h,t) = \frac{h^2}{3\eta}\nabla(\gamma\Delta h - \rho g h + \Pi(h)) + \frac{h}{2\eta}\nabla\gamma \tag{2}$$

the first term in the brackets is the Laplace pressure, the second one the hydrostatic contribution due to gravity, the third one the disjoining pressure. At the distance ℓ from the contact line, the disjoining pressure is negligible, and so is the hydrostatic contribution. The last term on the rhs is a surface tension gradient which requires a specific analysis, and will be ignored for the moment.

The equation for the angle is obtained by merely replacing the evaporation rate in the rhs by its value at the given distance $\ell \approx a\theta^{-2}$ from the contact line:

$$\frac{{\rm d}R}{{\rm d}t}\theta - \frac{\gamma}{3\eta}\theta^4 \approx -\frac{j_0}{\sqrt{2R\ell}} \approx -\frac{\theta j_0}{\sqrt{2Ra}}. \tag{10}$$

Table 1. Physical parameters of alkanes and water at 20 °C.

Liquid	Viscosity η ($\times 10^{-3}$ Pa s)	Surface tension γ ($\times 10^{-3}$ N m^{-1})	j_0 ($\times 10^{-10}$ m^2 s^{-1})
Hexane	0.326	18.4	34
Heptane	0.409	20.5	16
Octane	0.542	21.8	3.2
Nonane	0.711	24.2	1
Water (50% relative humidity)	1.002	72.8	2.6

For spherical caps, the general relation

$$\frac{\mathrm{d}V}{\mathrm{d}t} \approx -2\pi j_0 R, \tag{6}$$

valid as long as $R \gg \ell$, allows one to close the system.

The coupled equations can be solved if initial conditions are chosen. A relevant parameter is the radius R_0 at the maximum extension of the drop, i.e. $\frac{\mathrm{d}R}{\mathrm{d}t} = 0$. The contact angle is θ_0 and can be expressed as a function of the drop radius.

If ℓ is a constant,

$$\theta_0^4 \approx \frac{3\eta j_0}{\gamma\sqrt{2R_0\ell}}. \tag{11}$$

This accounts for situations where the rate-limiting step for evaporation at the contact line is the transfer rate of molecules across the liquid–vapour interface. If

$$\ell \approx a\theta^{-2}, \qquad \theta_0^3 \approx \frac{3\,\eta j_0}{\gamma\sqrt{2\,R_0\,a}}. \tag{12}$$

This is the case when the rate-limiting step for evaporation at the contact line is due to the disjoining pressure. The specific dependence $\ell \approx a\theta^{-2}$ results from (9).

Therefore, the present model allows us to express the contact angle at maximum extension as a function of the drop radius, and then to calculate the subsequent dynamics for both radius and contact angle. Note that even if ℓ (or a) is an external parameter, its meaning and order of magnitude are known.

The behaviour of equation (10) is controlled by the 'capillary' number:

$$C = \frac{3\eta j_0}{\gamma R_0\theta_0^4}. \tag{13}$$

Depending on the model, $C \approx \sqrt{\frac{2\ell}{R_0}}$ or $C \approx \sqrt{\frac{2a}{R_0\theta_0^2}}$, and therefore must be small with respect to unity.

3.2. Check again experiments

The physical parameters of water and alkanes at 20 °C can be found in table 1.

For a maximum radius $R_0 = 5$ mm and assuming $\ell = 0.1$ μm, typical values given by equation (11) are $\theta_0 = 0.015$ rad for octane and $\theta_0 = 0.013$ rad for water. The results are the same with equation (12) if $a = 0.1$ nm.

Experimental data for $R_0 = 5$ mm are $\theta_0 = 0.015$ rad for octane, in good agreement with the model, but 0.04 rad for water, which is less satisfactory. However, the mere ability of the

Table 2. Calculated values of the exponents y and x as a function of the parameter C for the two models investigated.

$\ell \approx a\theta^{-2}$		$C \approx \sqrt{\frac{2a}{R_0\theta_0^2}}$ (12)		$\ell \approx$ Cst.		$C \approx \sqrt{\frac{2\ell}{R_0}}$ (11)	
C	y	x	$2y+x$	C	y	x	$2y+x$
10^{-4}	0.54	−0.09	1	10^{-4}	0.53	−0.06	1
10^{-3}	0.54	−0.09	1	10^{-3}	0.53	−0.06	1
10^{-2}	0.54	−0.09	1	10^{-2}	0.53	−0.06	1
0.05	0.52	−0.07	1	0.05	0.52	−0.04	1
0.1	0.51	−0.04	1	0.1	0.52	−0.03	1
0.12	0.50	−0.01	1	0.12	0.51	−0.02	1
0.15	0.49	+0.06	1	0.15	0.50	0	1
0.20	0.48	+0.33	1.3	0.20	0.47	+0.04	1

model to predict values for the contact angle in the correct amplitude range is an interesting step.

While the predicted values for the contact angle are the same with (11) or (12) for $\ell = 0.1\ \mu$m, $a = 0.1$ nm, and $R_0 = 5$ mm, this is no longer the case if the initial volume of the drop, and consequently the maximum radius, is changed. From (11), $\theta_0 \propto R_0^{-1/8}$, while from (12), $\theta_0 \propto R_0^{-1/6}$. The experiment should allow us to choose between these assumptions. However, the experimental dependence is rather $\theta_0 \propto R_0^{-0.45}$ [27], which disagrees with both models.

The disagreement between calculated and measured dependences has consequences for the resolution of equation (10), which has to be kept self-consistent. If θ_0 is defined as being the angle where the radius is a maximum, then conversely ℓ and a are given by (11) and (12) respectively. The behaviour of the equation is still controlled by the number

$$C = \frac{3\eta j_0}{\gamma\, R_0\, \theta_0^4}$$

known from experiment, and from which ℓ and a are now deduced.

The predicted dynamics, obtained by solving the system of coupled equations (8) and (10), is summarized in table 2 which needs some comments. In order to draw log–log plots as a function of the time interval $t_0 - t$, the time t_0 has to be defined in a relevant way i.e., by an extrapolation of the points where $R \gg \ell$, and not by the time where the calculated radius vanishes. Well defined power laws are obtained for the radius. For the angle, power laws are acceptable for small C but deteriorate above 0.15. Typical results are plotted in figure 5.

If $\ell \approx a\theta^{-2}$, C is given by (12). The relation $2\,y + x = 1$ is obeyed till $C \approx 0.16$, above which the model loses validity, because $a\,\theta^{-2}$ rapidly becomes of order R.

The exponent y is slightly less than 0.5 for $C > 0.12$.

This accounts fairly well for the behaviour of alkanes, where the values of C calculated from the measured values of R_0 and θ_0 are in the range 0.12 for nonane to 0.16 for hexane. This would correspond to calculated values for the exponent between 0.48 and 0.50, while the experimental values of the exponent are $0.44 \leqslant y \leqslant 0.48$.

The exponent y is larger than 0.5 for $C < 0.12$, and saturates at the value $6/11 = 0.54$ for small C. In this limit, the first term in equation (10) has become negligible.

The experimental value for C is 8×10^{-4} in water, which corresponds to a calculated value $y = 0.54$, while the experimental value is $y = 0.57$. However, difficulties remain in this case, because the value of the parameter a is 2.6×10^{-11} m, a quarter of an Angström, which is unacceptably small.

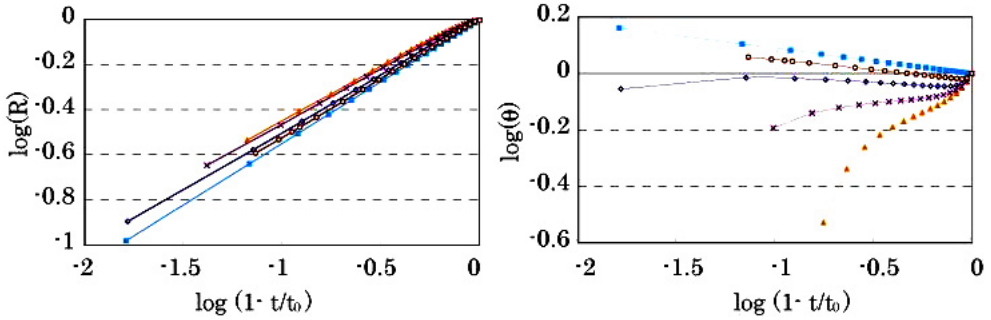

Figure 5. Calculated radius and contact angle for different C values in logarithmic (decimal) representation, in the case where $\ell \approx a\,\theta^2$. The values of y and x can be found in table 2. Cyan/square, $C = 0.001$; maroon/circle, $C = 0.05$; blue/diamond, $C = 0.1$; purple/cross, $C = 0.15$; orange/triangle, $C = 0.2$.

The results are slightly farther from the experimental trends if the length ℓ is taken as a constant. In fact, experiment would suggest that even in equation (10) the angular dependence of the rhs is underestimated. Other shapes for the disjoining pressure would lead to a better agreement, but we shall refrain from introducing 'ad hoc' procedures.

3.3. Discussion

The models presented above assume stationary, diffusion driven evaporation. The specific problem at the contact line is treated empirically, but using physical arguments relevant for the system considered. The results are globally fairly good, which supports well the main assumptions made, even if the evaporation term is not perfectly treated.

However, the case of water is intriguing. Noticeably, the contact angle at the maximum drop extension is three times larger than the one (experimental as well as calculated) of octane, which has a similar evaporation rate. This corresponds to a unrealistic value of the parameter a, and requires us to question further both theory and experiments.

- As no contact line pinning is observed during the receding motion, the hypothesis of an incomplete wetting of the substrate, which would increase the contact angle, is not very plausible. Actually, defects are always present on silica, and a stick–slip behaviour would be expected in partial wetting.
- Another hypothesis deals with the disjoining pressure of water on silica, which exhibits a non-monotonic behaviour [32], therefore not obeying (9). This is certainly the cause of the specific behaviour of water drops in the last stage. Further work is needed to check if taking into account a realistic shape for the disjoining pressure of water could explain the large values of the angles during the whole retraction.

Whatever the liquid considered, one question has not been answered. The previous analysis assumes that the temperature of the drop is uniform. This is why the last term in equation (2) has been ignored.

$$U(h,t) = \frac{h^2}{3\eta}\nabla(\gamma\Delta h - \rho g h + \Pi(h)) + \frac{h}{2\eta}\nabla\gamma. \tag{2}$$

As heat transfer is associated with evaporation, which is not uniform over the drop, the question must be raised. However, the effects are expected to be weak, because the drops are

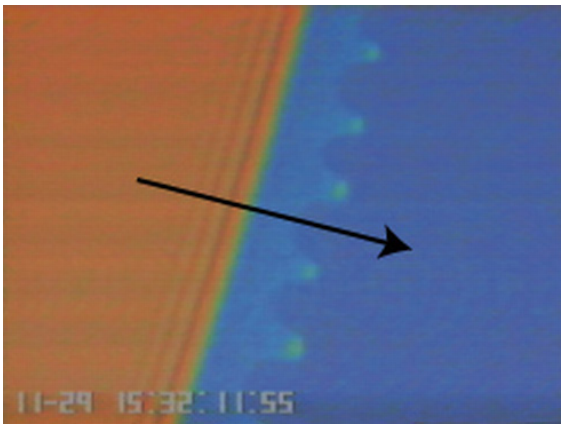

Figure 6. Surface-tension driven film instabilities during the advancing motion (spreading) of an octane drop on a silicon wafer. The drop (orange) is on the left, the bare substrate (blue) on the right. The substrate used is a silicon wafer with a thick layer of silica (typically 100 nm) which enhances the optical contrast and allows us to see the film (blue-green). This also explains the (true) colours seen on the picture.

very thin, and thermally induced gradients are much smaller than solutal ones (as would be the case in mixtures).

4. Thermally induced surface tension gradients

4.1. Temperature distribution in an evaporating drop

How the temperature is distributed in an evaporating drop raises questions quite similar to the ones encountered above in the discussion of the evaporation process.

The maximum thicknesses observed during the receding motion are always less than 50 μm, while the thermal diffusion coefficient D_{th} of the liquids considered is typically 10^{-7} m^2 s^{-1}. Therefore characteristic times are less than 0.03 s, which should ensure that a stationary, diffusion controlled distribution of temperatures is reached during the receding motion.

However, when the advancing motion (spreading) is considered, the conclusion is not so straightforward. Experiments [33, 34] provide evidence of an outwardly directed surface tension gradient during the spreading of volatile drops. This is illustrated in figure 6. As the surface tension decreases with increasing temperature, what figure 6 means is that during spreading the edge of the drop is colder than the centre, and noticeably not at the temperature of the substrate, which would be the case in a stationary situation.

Looking forward to the experiment, one observes that the drops stay some time at the maximum extension before receding. During this time interval, the contact angle decreases, i.e., the drop becomes thinner, and the film giving evidence of the surface tension gradient fades out. This time is short for the most volatile liquids ($\approx$1 s for hexane) and longer with nonane or water ($\approx$20 s).

This suggests that a stationary temperature distribution is probably established as soon as the drop starts to recede, controlled by thermal diffusion, and therefore obeying $\Delta T = 0$. As the drops are very flat, this becomes $\frac{\partial^2 T}{\partial z^2} = 0$ where z is the vertical direction. This means that the temperature varies linearly over the drop thickness. It is equal to the temperature T_0 of the

substrate at the bottom and decreases with height inside the liquid. More precisely [16],

$$T(h) = T_0 \left[1 - \frac{L J(h)}{T_0 \kappa} h \right] \tag{14}$$

where L is the latent heat and κ the thermal conductivity. Note that whatever the way $J(r)$ behaves at the edge of the drop, the product $h(r)J(r)$ tends to zero, at least for spherical caps or similar profiles. The surface tension gradient is now oriented inwards.

4.2. Consequences on the dynamics

- Let us first comment about the value of the maximum radius R_0 reached at the end of the spreading process, during which an outwardly directed surface tension gradient is present. Then the radius increases faster than in an isothermal process. On the other hand, the global evaporation rate, which is proportional to the radius, increases also. Therefore, the experimental values R_0 and θ_0 are not necessarily relevant parameters for the theoretical analyses. Noticeably, the disagreement between the experimental relation $\theta_0 \propto R_0^{-0.45}$ and the model could be irrelevant. The question is still open.
- Second, during retraction and assuming (14) to hold, there will be (i) a coupling between local temperature and evaporation rate [16] and (ii) a contribution of the 'Marangoni' velocity $\frac{h}{2\eta}\nabla\gamma$ in the drop dynamics. In the present case, i.e., with very thin drops, the second term in the brackets of equation (14) is small. More precisely, it is less than 3×10^{-4} for a water drop 50 μm thick, and ten times larger with hexane. Therefore, we do not expect an observable effect of temperature gradients, at least if the assumption of stationarity holds during retraction.

In conclusion, we believe that temperature gradients are negligible during the drop retraction, but that the relevance of the experimental values of R_0 and θ_0 is questionable.

Even if this does not play a role in our thin drops, it is interesting to note that alkanes and water have very different responses to temperature gradients.

It is reported that Marangoni flow is quite effective in alkanes, either with sessile drops on a heated substrate, or with drops hanging in a warmer gas phase [35–38]. Strong internal flows are commonly visualized with tracers when the contact angle is larger than 20° [35–38]. Infrared observations show that in this case the temperature rapidly becomes homogeneous over the drop [35].

The case of water is a long lasting story. No Marangoni flow was ever seen in the experiments reported [35–38], and stratified temperature distributions were observed in hanging drops [35]. Contamination of the free interface has been assumed by several authors [35–37], and denied by others [39]. What seems to be accepted is the assumption of some interface rigidity, reducing the surface flow in water.

5. General conclusion

The present paper proposes an up to date report on the problem of evaporating drops in the case of complete wetting, and presents new, well controlled experiments with water and alkanes. Available models are discussed, based on the assumption of an evaporation process driven by the stationary diffusion of vapour molecules in the gas phase. At present, an isothermal model, taking explicitly into account the specific properties of thin films, agrees well with the behaviour of simple liquids like alkanes, except for the relation between radius and contact angle at the maximum extension of the drop. The case of water requires further analyses,

possibly because the specific interaction of this polar liquid with hydrophilic substrates is not properly accounted for.

Acknowledgment

We gratefully acknowledge Ahmed Hamraoui, who provided us with ultrapure water.

References

[1] Maxwell J C 1877 *Diffusion—Collected Scientific Papers* (Cambridge: Encyclopedia Britannica)
[2] Langmuir I 1918 Evaporation of small spheres *Phys. Rev.* **12** 368
[3] Fuchs N A 1959 *Evaporation and Droplet Growth in Gaseous Media* ed R S Bradley (Oxford: Pergamon)
[4] Frohn A and Roth N 2000 *Dynamics of Droplets* (Berlin: Springer)
[5] Morse H W 1910 *Proc. Am. Acad. Sci.* **45** 363
[6] Topley B and Whytlaw-Gray R 1927 *Phil. Mag.* **4** 873
[7] Houghton H G 1933 *Physics* **4** 419
[8] Roth N, Anders K and Frohn A 1993 Size and evaporation rate measurements of optically levitated droplets *Proc. 3rd Int. Congr. on Optical Particle Sizing* p 371
[9] Ranz W E and Marshall W R 1952 *Chem. Ing. Prog.* **48** 173
[10] Deegan R D, Bakajin O, Dupont T F, Huber G, Nagel S R and Witten T A 1997 *Nature* **389** 827
[11] Deegan R D 2000 *Phys. Rev.* E **61** 475
[12] Deegan R D, Bakajin O, Dupont T F, Huber G, Nagel S R and Witten T A 2000 *Phys. Rev.* E **62** 757
[13] Miladinova S, Slatchev S, Lebon G and Legros J C 2002 *J. Fluid Mech.* **453** 153
[14] Kim I Y and Wayner P C 1996 *J. Thermophys. Heat Transfer* **10** 320
[15] Wayner P C 1993 *Langmuir* **9** 924
[16] Sultan E, Boudaoud A and Ben Amar M 2005 *J. Fluid Mech.* **543** 183
[17] Popov Y O and Witten T A 2001 *Eur. Phys. J.* E **6** 211
[18] Jackson J D 1975 *Classical Electrodynamics* 2nd edn (New York: Wiley)
[19] Crank J 1975 *The Mathematics of Diffusion* 2nd edn (Oxford: Oxford University Press)
[20] Hocking L M 1995 *Phys. Fluids* **7** 2950
[21] Morris S J S 2001 *J. Fluid Mech.* **432** 1
[22] Anderson D M and Davis S H 1995 *Phys. Fluids* **7** 248
[23] Qu D, Ramé E and Garoff S 2002 *Phys. Fluids* **14** 1154
[24] Cachile M, Bénichou O and Cazabat A M 2002 *Langmuir* **18** 7985
[25] Cachile M, Bénichou O, Poulard C and Cazabat A M 2002 *Langmuir* **18** 8070
[26] Poulard C, Bénichou O and Cazabat A M 2003 *Langmuir* **19** 8828
[27] Poulard C, Guéna G, Cazabat A M, Boudaoud A and Ben Amar M 2005 *Langmuir* **21** 8226
[28] Vig J R 1985 *J. Vac. Sci. Technol.* A **3** 1027
[29] Derjaguin B V, Churaev N V and Muller V M 1987 *Surface Forces* (New York: Cons. Bureau)
[30] Israelachvili J 1991 *Intermolecular and Surface Forces* 2nd edn (New York: Academic)
[31] de Gennes P G 1985 Wetting: statics and dynamics *Rev. Mod. Phys.* **57** V3, 827
[32] Derjaguin B V and Zorin Z M 1955 *Zh. Fiz. Khim.* **29** 1755
[33] Redon C, Brochard-Wyart F and Rondelez F 1992 *J. Physique* II **2** 580
[34] Bénichou O, Cachile M, Cazabat A M, Poulard C, Valignat M P, Vandenbrouck F and Van Effenterre D 2003 *Adv. Colloid Interface Sci.* **100–102** 381
[35] Savino R, Paterna D and Favaloro N 2002 *J. Thermodyn. Heat Transfer* **16** 562
[36] Hegseth J J, Rashidnia N and Chai A 1996 *Phys. Rev.* E **54** 1640
[37] Zhang N and Chao D F 2001 *J. Flow Vizualisation Image Process.* **8** (2–3)
[38] Hu H and Larson R G 2005 *Langmuir* **21** 3963
[39] Ward C A and Stanga D 2001 *Phys. Rev.* E **64** 051509